

---

# Compile Scene Graphs with Reinforcement Learning

---

Zuyao Chen<sup>1,2</sup> Jinlin Wu<sup>3,4</sup> Zhen Lei<sup>3,4</sup> Marc Pollefeys<sup>2,5</sup> Chang Wen Chen<sup>1</sup>

<sup>1</sup>The Hong Kong Polytechnic University <sup>2</sup>ETH Zürich <sup>3</sup>CAIR, HKISI-CAS

<sup>4</sup>Institute of Automation, CAS <sup>5</sup>Microsoft

## Abstract

Next token prediction is the fundamental principle for training large language models (LLMs), and reinforcement learning (RL) further enhances their reasoning performance. As an effective way to model language, image, video, and other modalities, the use of LLMs for end-to-end extraction of structured visual representations, such as scene graphs, remains underexplored. It requires the model to accurately produce a set of objects and relationship triplets, rather than generating text token by token. To achieve this, we introduce *R1-SGG*, a multimodal LLM (M-LLM) initially trained via supervised fine-tuning (SFT) on the scene graph dataset and subsequently refined using reinforcement learning to enhance its ability to generate scene graphs in an end-to-end manner. The SFT follows a conventional prompt-response paradigm, while RL requires the design of effective reward signals. We design a set of graph centric rewards, including three recall based variants—Hard Recall, Hard Recall+Relax, and Soft Recall—which evaluate semantic and spatial alignment between predictions and ground truth at the object and relation levels. A format consistency reward further ensures that outputs follow the expected structural schema. Extensive experiments on the VG150 and PSG benchmarks show that R1-SGG substantially reduces failure rates and achieves strong performance in Recall and mean Recall, surpassing traditional SGG models and existing multimodal language models.

## 1 Introduction

Scene graphs, as structured visual representations, have gained increasing attention in many vision applications, such as robot manipulation [44, 41], robot navigation [7, 23, 37], and medical image or video analysis [20, 24], *etc*. To generate scene graphs from an image, traditional Scene Graph Generation (SGG) models [10, 34, 14, 38, 29, 2, 15, 11, 5, 40, 4] decouple the task into two subtasks, *i.e.*, object detection and visual relationship recognition, and directly maximize the likelihood of the ground-truth labels given the image. Essentially, these models tend to overfit the distribution of annotated datasets; Consequently, they struggle to handle long-tail distributions and are prone to generating biased scene graphs (*e.g.*, all predicted relationships are head classes like “on” and “of”).

While traditional SGG models rely on manual annotated datasets and struggle to generalize to new domains, recent advances in large language models (LLMs) offer a new paradigm. LLM4SGG [12] utilizes an LLM to extract relationship triplets from captions using both original and paraphrased text, while GPT4SGG [3] employs an LLM to synthesize scene graphs from dense region captions. Additionally, Li [17] generates scene graphs via image-to-text generation using vision-language models (VLMs). These weakly supervised methods demonstrate potential for generating scene graphs with little or no human annotation but suffer from accuracy issues in the generated results.

Despite these advancements, existing methods typically employ text-only LLMs or rely on intermediate captions as input, which do not fully leverage the rich visual context. In contrast, multimodal large language models (M-LLMs) which integrate both visual and linguistic modalities offer the potential for more direct and holistic scene understanding. By processing visual information alongside

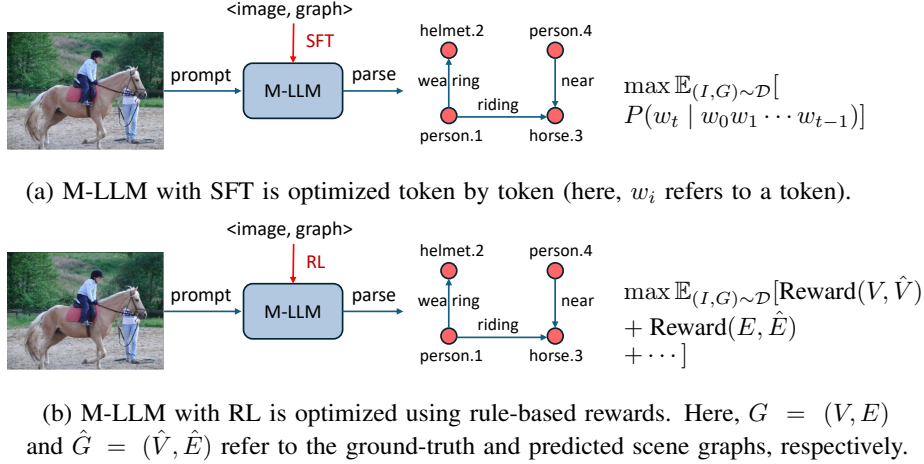


Figure 1: Comparison of multimodal LLMs (M-LLMs) fine-tuned via Supervised Fine-tuning (SFT) and Reinforcement Learning (RL) for Scene Graph Generation (SGG).

natural language prompts, M-LLMs can generate scene graphs in an end-to-end manner. However, in practice, M-LLMs suffer from instruction following (*e.g.*, the output does not contain “objects” or “relationships”), repeated response (*e.g.*, `{"objects": [... {"id": "desk.9", "bbox": [214, 326, 499, 389]}, {"id": "desk.10", "bbox": [214, 326, 499, 389]}, {"id": "desk.11", "bbox": [214, 326, 499, 389]}, ... ] ... }`), inaccurate location, *etc*. These challenges highlight the need for better alignment between visual understanding and structured representation within the M-LLM framework.

To improve instruction-following and structured output generation in M-LLMs, one intuitive solution is to perform Supervised Fine-tuning (SFT) on scene graph datasets (see Fig. 1-(a)). In the context of SGG, SFT aligns the model’s outputs with expected formats (*e.g.*, structured lists of objects and relationships) by training it on high-quality scene graph annotations. This process encourages the model not only to recognize entities and relations from the image but also to organize them into a coherent and valid graph structure. Nevertheless, SFT alone still be insufficient as all output tokens are weighted equally in the loss. For example, the experimental results on the VG150 dataset [34] reveal that even with SFT, M-LLM still has a high failure rate to generate a valid and high-quality scene graph. The drawback of SFT in SGG lies in the lack of effective signals to correct the output (*e.g.*, the model cannot directly utilize the Intersection over Union (IoU) between the predicted box and the ground truth to refine its output).

To advance M-LLMs for effective Scene Graph Generation (SGG), we propose *R1-SGG*, a novel framework leveraging visual instruction tuning enhanced by reinforcement learning (RL). The visual instruction tuning stage follows a conventional supervised fine-tuning (SFT) paradigm, *i.e.*, fine-tuning the model using prompt-response pairs with a cross-entropy loss. For the RL stage, we adopt GRPO, an online policy optimization algorithm introduced in DeepSeekMath [28].

To enable effective reinforcement learning for Scene Graph Generation, we introduce a set of rule-based, graph-centric rewards that reflect the structural characteristics of scene graphs. Given an image and a prompt, a multimodal large language model (M-LLM) generates a set of objects and relational triplets. To evaluate and optimize these predictions, we formulate reward functions aligned with standard SGDET metrics [34] and structured reasoning objectives. Specifically, we define three reward variants: **Hard Recall**, which counts a triplet as correct only if the subject, predicate, and object labels exactly match the ground truth and both bounding boxes achieve  $\text{IoU} > 0.5$ ; **Hard Recall+Relax**, which relaxes the exact match constraint by incorporating embedding similarity between predicted and ground-truth labels; and **Soft Recall**, which further densifies reward signals via bipartite matching, combining object label similarity,  $\text{IoU}$ , and bounding box distance into a unified cost function. These scene graph rewards are computed over matched object and edge pairs, and are complemented by a format reward that enforces structural adherence in output formatting. This reward design enables stable and fine-grained policy optimization using GRPO, guiding the M-LLM toward generating accurate, complete, and structurally valid scene graphs.

Our contributions can be summarized as follows:

- We explore how to develop a multimodal LLM for Scene Graph Generation (SGG), by leveraging visual instruction tuning with reinforcement learning (RL). To our knowledge, this is a pioneer work that develops a multimodal LLM to generate scene graphs in an end-to-end manner.
- Graph-centric, rule-based rewards are designed to guide policy optimization in a manner aligned with standard evaluation metrics in SGG, such as the recall of relationship triplets—metrics that cannot be directly optimized through SFT.
- Experimental results demonstrate that the proposed framework improves the ability to understand and reason about scene graphs for multimodal LLMs.

## 2 Related Work

**Scene Graph Generation (SGG).** Scene Graph Generation (SGG) is a foundational task in structured visual understanding, where the goal is to represent an image as a graph of objects and their pairwise relationships. Traditional approaches like [34, 14, 38, 29, 2, 15, 11, 5] decouple the task into object detection and relationship classification stages, and are typically trained via supervised learning on datasets such as Visual Genome (VG150) [34]. While effective, these models are limited by their reliance on annotated data and exhibit strong bias toward head predicates such as “on” or “of”, struggling on long-tail classes.

To overcome the closed-set limitation, recent work has explored open-vocabulary SGG. For example, OvSGTR [4] extends scene graph prediction to a fully open-vocabulary setting by leveraging visual-concept alignment. In parallel, weakly supervised methods have been developed to reduce the annotation burden. These approaches, such as those proposed by [43, 16, 40, 4], use image-caption pairs as supervision to distill relational knowledge, enabling generalization to unseen concepts.

**LLMs for Scene Graph Generation.** With the rise of LLMs, several studies have attempted to synthesize scene graphs from natural language. LLM4SGG [12] extracts relational triplets from both original and paraphrased captions using text-only LLMs. GPT4SGG [3] goes a step further by using GPT-4 to generate scene graphs from dense region captions, improving contextual consistency and coverage. Meanwhile, [17] leverage vision-language models (VLMs) to produce scene graphs through image-to-text generation pipelines.

However, these caption-based or LLM-driven methods often exhibit limited accuracy, including incomplete object sets, and inconsistent relationship descriptions. These issues arise from the lack of structure in the generated outputs and the absence of mechanisms to refine the results according to scene-level constraints.

**Reinforcement Learning (RL) for LLMs.** Reinforcement learning (RL) has been increasingly adopted to enhance the reasoning capabilities of large models. Algorithms like Proximal Policy Optimization (PPO) [27] and Group Relative Policy Optimization (GRPO) [28] guide models using reward signals instead of relying solely on maximum likelihood estimation. In the context of large language models, DeepSeek-R1 [8] demonstrates that RL can significantly improve structured reasoning and planning.

In multimodal learning, however, RL remains underutilized for generating structured outputs. Our work addresses this by introducing rule-based reward functions at multiple levels, including three scene graph reward variants and a format consistency reward. These signals promote the generation of meaningful and coherent scene graphs by explicitly evaluating alignment with ground-truth annotations.

## 3 Methodology

### 3.1 Preliminary

**Scene Graph Generation (SGG).** Scene graph generation (SGG) transforms an image  $I$  into a structured representation that captures both objects and their interactions. Specifically, SGG produces

a directed graph  $\mathcal{G} = (\mathcal{V}, \mathcal{E})$ , where each node  $v_i \in \mathcal{V}$  represents an object annotated with an object category  $c_i$  and a bounding box  $b_i$ . Each relationship triplet  $e_{ij} \in \mathcal{E}$  captures the relationship between two nodes. The triplet is defined as  $e_{ij} := \langle v_i, p_{ij}, v_j \rangle$ , where  $p_{ij}$  encodes the visual relationship between the subject  $v_i$  and the object  $v_j$ , such as spatial relations (e.g., “on”, “under”) or interactive relations (e.g., “riding”, “holding”). Typically, SGG models decouple this task into two subtasks, namely object detection and relationship recognition, both optimized by maximizing the likelihood of the corresponding ground-truth labels given the image.

**Reinforcement Learning with GRPO.** Group Relative Policy Optimization (GRPO) is a online reinforcement learning algorithm introduced by DeepSeekMath [28]. Unlike traditional methods such as PPO [27], which require an explicit critic network, GRPO instead compares groups of candidates to update the policy  $\pi_\theta$ . Specifically, for each input query  $q$ , a set of candidate outputs  $\{o_i\}_{i=1}^G$  is drawn from the previous policy  $\pi^{\text{old}}(O|q)$ , and the advantage of each candidate is computed relative to the group’s average reward:

$$A_i = \frac{r_i - \text{mean}(\{r_1, \dots, r_G\})}{\text{std}(\{r_1, \dots, r_G\})}. \quad (1)$$

The policy parameters  $\theta$  are updated by maximizing the following GRPO objective:

$$J_{\text{GRPO}}(\theta) = \mathbb{E}_{q \sim P(Q), \{o_i\}_{i=1}^G \sim \pi^{\text{old}}(O|q)} \left[ \frac{1}{G} \sum_{i=1}^G \left( \min \left( \frac{\pi_\theta(o_i|q)}{\pi^{\text{old}}(o_i|q)} A_i, \right. \right. \right. \\ \left. \left. \left. \text{clip} \left( \frac{\pi_\theta(o_i|q)}{\pi^{\text{old}}(o_i|q)}, 1 - \epsilon, 1 + \epsilon \right) A_i \right) - \beta D_{\text{KL}}(\pi_\theta \parallel \pi_{\text{ref}}) \right], \quad (2)$$

Here,  $\epsilon$  and  $\beta$  are hyper-parameters. The first term uses a clipped probability ratio (as in PPO) to control the update magnitude, while the KL divergence regularizer  $D_{\text{KL}}(\pi_\theta \parallel \pi_{\text{ref}})$  constrains the new policy  $\pi_\theta$  to not deviate too much from a reference policy  $\pi_{\text{ref}}$ . This formulation, which combines a group-relative advantage, a clipping mechanism, and a KL divergence regularizer, stabilizes policy updates and improves training efficiency, demonstrating remarkable potential for enhancing the reasoning performance of LLMs such as DeepSeek R1 [8].

### 3.2 Overview of R1-SGG

R1-SGG is a reinforcement learning framework that enhances scene graph generation (SGG) in multimodal large language models (M-LLMs). It builds on a supervised fine-tuning (SFT) stage using prompt-response pairs, followed by reinforcement learning (RL) with structured, graph-centric rewards.

Given an input image and prompt, the M-LLM generates a scene graph  $\mathcal{G}_{\text{pred}} = (\mathcal{V}_{\text{pred}}, \mathcal{E}_{\text{pred}})$ , comprising objects (nodes) and their relationships (edges). We primarily optimize using *Hard Recall*, which aligns with SGDET metrics by rewarding exact triplet matches. To study the sparsity and design of the rewards, we also evaluated relaxed alternatives based on bipartite matching between  $\mathcal{G}_{\text{pred}}$  and the ground truth graph  $\mathcal{G}_{\text{gt}}$ , allowing fine-grained node and edge rewards. Our RL pipeline employs Group Relative Policy Optimization (GRPO) [28], which compares sampled outputs and promotes higher-reward candidates. By integrating SFT, GRPO, and graph-aware rewards, R1-SGG enables M-LLMs to generate accurate, diverse, and structurally valid scene graphs.

### 3.3 Rewards Definition

#### 3.3.1 Format Reward

Following DeepSeek R1 [8], we employ a format reward to ensure that the model’s response adheres to the expected structure, specifically `<think>...</think><answer>...</answer>`. A reward of 1 is assigned if the response follows this format and the segment enclosed by `<answer>...</answer>` contains both the keywords “object” and “relationships”; otherwise, the reward is 0.

#### 3.3.2 Scene Graph Rewards

Standard evaluation protocols for Scene Graph Generation (SGG), such as SGDET [34], formulate the task as a recall-oriented problem, emphasizing the model’s ability to retrieve correct relationship

triplets from an image. To investigate the impact of different reward formulations, we introduce three variants: *Hard Recall*, *Hard Recall+Relax*, and *Soft Recall*.

**Hard Recall.** To align policy optimization with standard SGDET metrics, we define *Hard Recall*, where a predicted triplet  $\langle \text{subject}, \text{predicate}, \text{object} \rangle$  is counted as a true positive when *both* of the following hold: 1) *Triplet accuracy*: the subject, predicate, and object labels exactly match the ground truth. 2) *Localization accuracy*: the IoU between predicted and ground-truth bounding boxes exceeds 0.5.

This reward is aligned with standard metrics but suffers from sparsity due to its strict criteria.

**Hard Recall + Relax.** We relax the triplet accuracy requirement by computing cosine similarity between the entity embeddings of predicted and ground-truth triplets. This softens the discrete matching constraint to provide more gradient signal.

**Soft Recall.** We further propose a dense matching reward by formulating it as a bipartite matching problem, similar to DETR [1], where predicted nodes  $\{v_i = (c_i, b_i)\}_{i=1}^M$  (each node  $v_i$  is comprising an object class  $c_i$  and a bounding box  $b_i$ ) are matched to ground-truth nodes  $\{\tilde{v}_j = (\tilde{c}_j, \tilde{b}_j)\}_{j=1}^N$  with the following cost:

$$\begin{aligned} \text{cost}(v_i, \tilde{v}_j) = & \lambda_1 \cdot (1.0 - \langle \text{Embedding}(c_i), \text{Embedding}(\tilde{c}_j) \rangle) \\ & + \lambda_2 \cdot (1.0 - \text{IoU}(b_i, \tilde{b}_j)) + \lambda_3 \cdot \|b_i - \tilde{b}_j\|_1, \end{aligned} \quad (3)$$

where  $\langle \cdot, \cdot \rangle$  denotes cosine similarity,  $\lambda_1, \lambda_2$  are weight factors, and *Embedding* is obtained via the NLP tool SpaCy. By solving the bipartite matching problem, we establish a one-to-one node matching between the predicted graph  $\mathcal{G}_{\text{pred}}$  and the ground-truth graph  $\mathcal{G}$ .

For a predicted node  $v_i$ , the reward is defined as

$$\text{Reward}(v_i) = \begin{cases} \lambda_1 \cdot \langle \text{Embedding}(c_i), \text{Embedding}(\tilde{c}_j) \rangle \\ \quad + \lambda_2 \cdot \text{IoU}(b_i, \tilde{b}_j) \\ \quad + \lambda_3 \cdot \exp(-\|b_i - \tilde{b}_j\|_1), & \text{if } v_i \text{ and } \tilde{v}_j \text{ are matched,} \\ 0, & \text{otherwise.} \end{cases} \quad (4)$$

which is the linear combination of object category similarity and the IoU of bounding boxes. The total rewards of an image's prediction set  $\{v_i\}_{i=1}^M$  is computed as

$$\text{Reward}(\{v_i\}_{i=1}^M) = \frac{1}{|\mathcal{V}_{\text{gt}}|} \sum_{i=1}^M \text{Reward}(v_i). \quad (5)$$

For a predicted triplet  $e_{ij} := \langle v_i, p_{ij}, v_j \rangle$ , the reward is defined as

$$\text{Reward}(e_{ij}) = \begin{cases} \langle \text{Embedding}(v_i), \text{Embedding}(\tilde{v}_k) \rangle \cdot \\ \langle \text{Embedding}(v_j), \text{Embedding}(\tilde{v}_l) \rangle \cdot \\ \langle \text{Embedding}(p_{ij}), \text{Embedding}(p_{kl}) \rangle, & \text{if } v_i \text{ matches } \tilde{v}_k \\ & \quad \text{and } v_j \text{ matches } \tilde{v}_l, \\ 0, & \text{otherwise.} \end{cases} \quad (6)$$

Thereby, the reward of an image's predicted edge set is computed as

$$\text{Reward}(\{e_{ij}\}) = \frac{1}{|\mathcal{E}_{\text{gt}}|} \sum \text{Reward}(e_{ij}). \quad (7)$$

## 4 Experiments

### 4.1 Dataset and Experiment Setup

**Dataset.** The widely-used scene graph dataset VG150 [34] consists of 150 object categories and 50 relation categories. Following prior works [40, 4], the training set used in this work contains

Table 1: SGDET performance on the VG150 validation set. For M-LLMs, predefined object classes and relation categories are included in the input prompts.

Method	Params	Failure Rate (%)	AP@50	Recall	mRecall
<i>Specific Models</i>					
IMP [34]			20.91	17.85	2.66
MOTIFS [38]	-	-	29.56	27.21	7.84
VCTree [29]			28.13	24.87	8.47
OvSGTR [4]			33.39	26.74	5.83
<i>Commercial M-LLMs</i>					
GPT-4o [9]	-	2.94	0.00	0.00	0.00
Gemini 1.5 Flash [25]	-	1.10	0.51	0.10	0.08
Gemini 2.0 Flash [6]	-	1.06	0.54	0.07	0.03
<i>Open-sourced M-LLMs</i>					
LLaVA v1.5 [21]	7B	82.70	0.00	0.00	0.00
Qwen2-VL-2B-Instruct [32]	2B	59.96	2.18	0.07	0.18
+SFT	2B	72.42	8.10	5.47	1.46
Qwen2-VL-7B-Instruct [32]	7B	54.46	6.07	0.69	0.80
+SFT	7B	39.54	14.18	9.62	3.30
R1-SGG-Zero	2B	0.34	12.30	11.89	5.70
R1-SGG	2B	0.10	17.87	21.09	7.48
R1-SGG-Zero	7B	0.04	15.59	18.34	8.32
R1-SGG	7B	<b>0.08</b>	<b>19.47</b>	<b>23.75</b>	<b>11.43</b>

56,224 image-graph pairs, while the validation set includes 5,000 pairs. To prompt the M-LLM, we transform each image-graph pair using the template described in Table 6.

The Panoptic Scene Graph (PSG) dataset [36] is built on the COCO dataset [18], consisting of 80 *thing* object categories, 53 *stuff* object categories, and 56 relation categories. It contains 46,563 image-graph pairs for training and 2,186 pairs for testing.

**Evaluation.** Following the standard evaluation pipeline in SGG, we adopt the SGDET protocol [34, 30] to measure the model’s ability to generate scene graphs. SGDET requires the model to generate scene graphs directly from the image without any predefined object boxes. Performance is evaluated using Recall and mean Recall (mRecall). Recall is computed for each image-graph pair, where a predicted triplet is considered correct if both the subject and object bounding boxes have an Intersection over Union (IoU) of at least 0.5 with the corresponding ground-truth boxes, and the subject category, object category, and relationship label all match the ground truth. Mean Recall (mRecall) is obtained by averaging the Recall across all relation categories. We additionally report AP@50 to assess object detection performance and Failure Rate to evaluate format consistency.

**Implementation Details.** Our code is based on the `tr1` library [31] and utilizes vLLM [13] to speed up sampling during reinforcement learning. For SFT, the model is trained for 3 epochs with a batch size of 128 on 4 NVIDIA A100 (80GB) GPUs, using the AdamW optimizer [22] with a maximum learning rate of 1e-5. For RL, the model is trained for 1 epoch with a batch size of 32 and 8 generations per sample on 16 NVIDIA GH200 (120GB) GPUs, also using AdamW with a maximum learning rate of 6e-7.

## 4.2 How Well Do M-LLMs Reason About Visual Relationships?

We evaluate the visual relationship reasoning capabilities of open-source multimodal LLMs using a four-to-one Visual Question Answering (VQA) task. Each model is prompted with an image and a corresponding question. The used prompt template is: Analyze the relationship between the object "`{sub_name}`" at `{sub_box}` and the object "`{obj_name}`" at `{obj_box}` in an image of size `{width}x{height}`. The bounding boxes are in `[x1, y1, x2, y2]` format. Choose the most appropriate relationship from the following options: A) `{choices[0]}`; B) `{choices[1]}`; C) `{choices[2]}`; D) `{choices[3]}`. We report Acc (accuracy over all questions) and mAcc (mean accuracy per image) in Table 7. The results reveal that many multimodal LLMs struggle with visual relationship reasoning. Moreover, the task exhibits a noticeable text bias, and the presence of bounding boxes can sometimes mislead the model’s attention. As a simpler task compared to SGG, the poor performance suggests that directly applying multimodal LLMs to SGG may yield suboptimal results.

### 4.3 How Well do M-LLMs Generate Scene Graphs?

#### 4.3.1 Benchmark on VG150

We report the performance under various settings in Table 1, which includes: 1) *Specific Models*: Methods built on specific detectors such as Faster R-CNN [26] (e.g., IMP [34]) or DETR [1] (e.g., OvSGTR [4]) for scene graph generation. 2) *Commercial M-LLMs*: Advanced multimodal large language models such as GPT-4o [9] and Gemini 1.5 Flash [25]. 3) *Open-source M-LLMs*: Publicly available models such as LLaVA v1.5 [21], Qwen2-VL [32], and our proposed *R1-SGG-Zero* (based on Qwen2-VL-2B/7B-Instruct, trained with GRPO but without supervised fine-tuning) and *R1-SGG* (built on the same backbone, fine-tuned with GRPO and initialized from SFT checkpoints).

The results in Table 1 reveal several key observations.

**Zero-shot Performance of M-LLMs.** Either commercial or open-source multimodal LLMs struggle to generate accurate scene graphs, and this can be attributed to several factors. First, the internal processing of private models such as GPT-4o remains opaque to users, resulting in suboptimal object detection performance. Second, models like LLaVA v1.5 align visual and textual features only at the image level, typically using a fixed resolution of  $336 \times 336$ , which restricts spatial understanding. Third, although models such as Gemini 2.0 and Qwen2-VL demonstrate a degree of spatial understanding, the task of scene graph generation is much complex than pure object detection or visual grounding. Consequently, their zero-shot performance drops significantly.

**SFT vs. RL.** 1) RL substantially improves performance across all metrics compared to SFT alone. Specifically, RL dramatically reduces the failure rate (e.g., from 72.42% to 0.10% for 2B models) and yields significant gains in AP@50, Recall, and mRecall. This highlights the effectiveness of GRPO in enhancing the model’s ability to generate accurate and complete scene graphs. 2) SFT achieves moderate improvements in AP@50 and Recall over the baseline but struggles with a relatively high failure rate. This suggests that SFT primarily improves relation prediction while being less effective at correcting structural errors, such as missing objects, relationships, or format inconsistencies. 3) applying RL on top of SFT (*i.e.*, R1-SGG) further boosts performance over both SFT and R1-SGG-Zero in most cases. This indicates that combining SFT and RL benefits from better initialization, leading to stronger relation recognition and higher recall. 4) larger models (e.g., 7B) consistently outperform smaller models (e.g., 2B) across AP@50, Recall, and mRecall, demonstrating the benefits of scaling model capacity for scene graph generation.

**Compared to Specific Models.** The gap between AP@50 and Recall highlights the advantage of dense predictions. However, our models, such as *R1-SGG*, achieve a notable mean Recall (mRecall) of 11.43%, suggesting that multimodal LLMs are more effective at generating less biased scene graphs. Moreover, specific models are typically restricted to a limited vocabulary and struggle to generalize across domains, whereas multimodal LLMs exhibit greater adaptability and broader generalization capabilities.

Overall, the results demonstrate that reinforcement learning (RL) significantly reduces the failure rate and enhances both object detection and relationship recognition. In contrast, supervised fine-tuning (SFT) alone results in a relatively high failure rate and limited improvements. As shown in Fig. 2, the failure rate quickly drops to near-zero with RL, whereas SFT continues to suffer from frequent structural errors.

#### 4.3.2 Benchmark on PSG

As shown in Table 2, our R1-SGG approach achieves strong performance on the PSG dataset. Compared to baselines, SFT significantly improves AP@50, Recall, and mean Recall (mRecall), while reinforcement learning further enhances relationship recognition, achieving the highest Recall (43.48% for 7B model) and mRecall (33.71%). Notably, our method also drives the failure rate to zero, demonstrating the effectiveness of reinforcement learning in promoting structured, accurate scene graph generation even without predefined object categories.

### 4.4 Qualitative Results

We present qualitative results in Fig. 6 and Fig. 7. As shown in Fig. 6, the ground-truth scene graph (Fig. 6-(a)) captures key objects and their relationships but is biased toward the predicate

Table 2: Performance on the PSG dataset [36]. For M-LLMs, predefined object classes and relation categories are included in the input prompts.

Model	Params	Failure Rate (%)	AP@50	Recall	mRecall
<i>Specific Models</i>					
IMP [34]				16.50	6.50
MOTIFS [38]				20.00	9.10
VCTree [29]	-	-	-	20.60	9.70
GPSNet [19]				17.80	7.00
PSGFormer [36]				18.60	16.70
<i>Open-sourced M-LLMs</i>					
LLaVA v1.5 [21]	7B	81.97	0.07	0.00	0.00
TextPSG [42]	-	-	-	4.80	-
ASMV2 [33]	13B	0.87	21.45	14.77	11.82
LLaVA-SpaceSGG [35]	13B	-	-	15.43	13.23
Qwen2-VL-2B-Instruct	2B	67.20	4.89	0.39	0.26
+SFT	2B	6.54	36.05	22.06	14.92
Qwen2-VL-7B-Instruct	7B	37.97	12.75	3.18	4.33
+SFT	7B	0.96	40.79	24.73	17.11
R1-SGG-Zero	2B	0.23	25.61	25.06	18.15
R1-SGG	2B	2.70	39.28	38.49	31.21
R1-SGG-Zero	7B	0.00	32.92	37.00	32.04
R1-SGG	7B	<b>0.00</b>	<b>42.05</b>	<b>43.48</b>	<b>33.71</b>

“has”. Conversely, the zero-shot Qwen2-VL-7B-Instruct (Fig. 6-(b)) fails to generate a valid JSON output, indicating poor instruction-following ability. With supervised fine-tuning, the model produces structurally valid graphs (Fig. 6-(c)) but frequently omits important relationships, resulting in a sparse scene graph. R1-SGG-Zero (7B), trained with RL only, improves relational recall and structure (Fig. 6-(d)), yet still outputs inaccurate triplets such as  $\langle \text{wheel}, \text{on}, \text{horse} \rangle$  and  $\langle \text{helmet.2}, \text{on}, \text{horse} \rangle$ . Finally, R1-SGG (7B), trained with both SFT and RL, produces a complete and consistent scene graph (Fig. 6-(e)), with results that even surpass the ground truth in relational richness.

#### 4.5 Discussion

Through the exploration of applying GRPO to the SGG task, we make several observations.

**KL Regularization.** We compare models trained with and without KL divergence regularization in Fig. 5. From the result, removing KL regularization leads to improved performance, particularly with a significant reduction in failure rate.

**Sampling Length.** In our experiments, the default sampling length is set to 1,024, which sufficiently covers most corrected answers. As shown in Fig. 5, increasing the sampling length to 2,048 does not yield further performance improvements, suggesting that longer sampling might enlarge the search space and introduce additional optimization difficulties without clear benefits. This observation aligns with prior findings on test-time scaling, where increasing Chain-of-Thought (CoT) length can degrade performance [39].

**Group Size.** As shown in Fig. 5, increasing the group size from 8 to 16 stabilizes training performance, consistent with the intuition that more candidates reduce variance in group statistics estimation. To balance computational cost and performance, we adopt a group size of 8 as the default in this work.

**To Think or Not Think?** We adopt the  $\langle \text{think} \rangle \dots \langle /think \rangle \langle \text{answer} \rangle \dots \langle /answer \rangle$  format in the system prompt, following DeepSeek R1 [8]. However, models such as Qwen2-VL-2B/7B-Instruct often fail to produce outputs with the  $\langle \text{think} \rangle$  tag after fine-tuning, indicating difficulty in adhering to the intended structure. This suggests that rule-based rewards alone are insufficient to trigger abstract reasoning patterns like CoT, and highlights the need for additional SFT on CoT-specific datasets to incentivize coherent intermediate reasoning.

**Generalization Across Datasets.** We report performance comparisons across datasets in Table 3. The results highlight several key insights: 1) **VG150 poses a significantly greater challenge than PSG**. For instance, SFT trained solely on PSG achieves a high AP@50 of 40.58 and Recall of 24.75%, with a low failure rate of 0.91%. In contrast, SFT trained only on VG150 results in a much higher failure rate of 39.54%, with notably lower AP@50 (14.18) and Recall (9.62%). 2) **SFT has a**

Table 3: Generalization across datasets using Qwen2-VL-7B-Instruct as the baseline. Columns under *Pre-training* indicate whether the weights were initialized from specific checkpoints, while the *Training* column specifies the dataset(s) used during the fine-tuning stage. “*w/o cats.*” denotes prompts without predefined object classes or relation categories.

Model	Pre-Training	Training	VG150				PSG			
			Failure Rate	AP@50	Recall	mRecall	Failure Rate	AP@50	Recall	mRecall
baseline	-	-	54.46	6.07	0.69	0.80	37.97	12.75	3.18	4.33
baseline ( <i>w/o cats.</i> )	-	-	44.58	6.83	0.61	0.37	30.28	13.79	1.96	2.30
SFT	-	VG150	39.54	14.18	9.62	3.30	22.10	11.05	3.03	1.36
SFT ( <i>w/o cats.</i> )	-	VG150	42.98	13.03	8.94	2.47	19.81	12.15	3.87	1.81
R1-SGG-Zero	-	VG150	0.04	15.59	18.34	8.32	<b>0.18</b>	<b>24.92</b>	<b>13.83</b>	<b>8.90</b>
R1-SGG-Zero ( <i>w/o cats.</i> )	-	VG150	0.06	15.30	16.33	6.94	0.18	18.10	6.16	3.38
R1-SGG	SFT	VG150	<b>0.08</b>	<b>19.47</b>	<b>23.75</b>	<b>11.43</b>	0.23	18.12	9.10	5.13
R1-SGG ( <i>w/o cats.</i> )	SFT ( <i>w/o cats.</i> )	VG150	0.30	18.09	22.73	9.62	0.64	14.64	7.51	3.88
SFT	-	PSG	36.98	5.79	1.42	0.77	0.91	40.58	24.75	17.31
SFT ( <i>w/o cats.</i> )	-	PSG	2.54	7.94	1.77	1.25	1.01	39.02	23.70	17.17
R1-SGG-Zero	-	PSG	<b>0.12</b>	<b>14.22</b>	<b>8.90</b>	<b>5.34</b>	0.00	32.92	37.00	32.04
R1-SGG-Zero ( <i>w/o cats.</i> )	-	PSG	0.02	9.08	2.80	1.78	0.05	24.26	19.94	18.04
R1-SGG	SFT	PSG	0.94	10.38	4.40	2.69	<b>0.00</b>	<b>42.05</b>	<b>43.48</b>	<b>33.71</b>
R1-SGG ( <i>w/o cats.</i> )	SFT ( <i>w/o cats.</i> )	PSG	0.14	9.38	2.16	1.55	0.14	41.15	41.44	31.51

Table 4: Ablation of reward formulations on VG150 validation set using R1-SGG (7B).

Setting	Sparsity	Metric Aligned	Failure Rate (%)	AP@50	Recall (%)	mRecall (%)
Hard Recall	sparse	✓	0.08	19.47	23.75	11.43
Hard Recall + Relax	medium	✗	0.02	19.93	24.05	9.61
Soft Recall	dense	✗	0.06	18.73	21.92	5.61

**strong domain-specific effect.** SFT models trained on one dataset (*e.g.*, VG150) exhibit substantial performance drops when evaluated on another (*e.g.*, PSG), reflecting limited transferability. For example, VG150-trained SFT only achieves 3.03% Recall and 1.36% mRecall on PSG. 3) **Predefined categories in the prompt.** Models trained and evaluated without categories (denoted as “*w/o cats.*”) generally exhibit a slight drop in performance, while those with category information demonstrate better generalization under open-set settings. 4) **Initialization of RL matters.** R1-SGG initialized with SFT checkpoints consistently outperforms R1-SGG-Zero. On VG150, R1-SGG (7B) achieves 23.75% Recall and 11.43% mRecall versus 18.34% and 8.32% for R1-SGG-Zero. A similar trend is observed on PSG. This highlights the importance of using SFT as a warm-start for reinforcement learning, which leads to improved sample efficiency and stronger downstream performance. 5) **R1-SGG-Zero exhibits stronger cross-dataset generalization.** This aligns with the domain-specific nature of SFT—models trained via SFT tend to overfit to the source domain, resulting in degraded performance on unseen datasets. In contrast, R1-SGG-Zero, trained without SFT, generalizes more robustly across domains.

**Hard Recall vs. Soft Recall.** As shown in Table 4, *Hard Recall* outperforms other variants despite providing sparser reward signals. This highlights the importance of aligning reward functions with evaluation metrics, rather than prioritizing reward smoothness alone.

## 5 Conclusion

We present a reinforcement learning framework for enhancing end-to-end Scene Graph Generation (SGG) with multimodal large language models (M-LLMs). To align training with the structured nature of scene graphs, we design a set of rule-based rewards, comprising three scene graph variants (*Hard Recall*, *Hard Recall+Relax*, and *Soft Recall*) and a format consistency reward, which enable fine-grained and stable policy optimization via GRPO. Our approach significantly improves the structural validity and relational accuracy of generated scene graphs. We release our code and models to support future research on structured visual understanding with M-LLMs.

## References

[1] Nicolas Carion, Francisco Massa, Gabriel Synnaeve, Nicolas Usunier, Alexander Kirillov, and Sergey Zagoruyko. End-to-end object detection with transformers. In *ECCV*, pages 213–229, 2020.

[2] Tianshui Chen, Weihao Yu, Riquan Chen, and Liang Lin. Knowledge-embedded routing network for scene graph generation. In *CVPR*, pages 6163–6171, 2019.

[3] Zuyao Chen, Jinlin Wu, Zhen Lei, Zhaoxiang Zhang, and Changwen Chen. GPT4SGG: Synthesizing scene graphs from holistic and region-specific narratives. *arXiv preprint arXiv:2312.04314*, 2023.

[4] Zuyao Chen, Jinlin Wu, Zhen Lei, Zhaoxiang Zhang, and Chang Wen Chen. Expanding scene graph boundaries: fully open-vocabulary scene graph generation via visual-concept alignment and retention. In *ECCV*, pages 108–124, 2024.

[5] Yuren Cong, Michael Ying Yang, and Bodo Rosenhahn. Reltr: Relation transformer for scene graph generation. *IEEE Trans. Pattern Anal. Mach. Intell.*, 45(9):11169–11183, 2023.

[6] Google AI for Developers. Gemini 2.0 flash. <https://ai.google.dev/gemini-api/docs/models#gemini-2.0-flash>, 2025.

[7] Qiao Gu, Ali Kuwajerwala, Sacha Morin, Krishna Murthy Jatavallabhula, Bipasha Sen, Aditya Agarwal, Corban Rivera, William Paul, Kirsty Ellis, Rama Chellappa, et al. Conceptgraphs: Open-vocabulary 3d scene graphs for perception and planning. In *ICRA*, pages 5021–5028, 2024.

[8] Daya Guo, Dejian Yang, Haowei Zhang, Junxiao Song, Ruoyu Zhang, Runxin Xu, Qihao Zhu, Shirong Ma, Peiyi Wang, Xiao Bi, et al. Deepseek-r1: Incentivizing reasoning capability in llms via reinforcement learning. *arXiv preprint arXiv:2501.12948*, 2025.

[9] Aaron Hurst, Adam Lerer, Adam P Goucher, Adam Perelman, Aditya Ramesh, Aidan Clark, AJ Ostrow, Akila Welihinda, Alan Hayes, Alec Radford, et al. Gpt-4o system card. *arXiv preprint arXiv:2410.21276*, 2024.

[10] Justin Johnson, Ranjay Krishna, Michael Stark, Li-Jia Li, David Shamma, Michael Bernstein, and Li Fei-Fei. Image retrieval using scene graphs. In *CVPR*, pages 3668–3678, 2015.

[11] Siddhesh Khandelwal and Leonid Sigal. Iterative scene graph generation. In Sanmi Koyejo, S. Mohamed, A. Agarwal, Danielle Belgrave, K. Cho, and A. Oh, editors, *NeurIPS*, 2022.

[12] Kibum Kim, Kanghoon Yoon, Jaehyeong Jeon, Yeonjun In, Jinyoung Moon, Donghyun Kim, and Chanyoung Park. Llm4sgg: Large language model for weakly supervised scene graph generation. *arXiv e-prints*, pages arXiv–2310, 2023.

[13] Woosuk Kwon, Zhuohan Li, Siyuan Zhuang, Ying Sheng, Lianmin Zheng, Cody Hao Yu, Joseph E. Gonzalez, Hao Zhang, and Ion Stoica. Efficient memory management for large language model serving with pagedattention. In *Proceedings of the ACM SIGOPS 29th Symposium on Operating Systems Principles*, 2023.

[14] Yikang Li, Wanli Ouyang, Bolei Zhou, Kun Wang, and Xiaogang Wang. Scene graph generation from objects, phrases and region captions. In *ICCV*, pages 1270–1279, 2017.

[15] Rongjie Li, Songyang Zhang, and Xuming He. Sgtr: End-to-end scene graph generation with transformer. In *CVPR*, pages 19464–19474, 2022.

[16] Xingchen Li, Long Chen, Wenbo Ma, Yi Yang, and Jun Xiao. Integrating object-aware and interaction-aware knowledge for weakly supervised scene graph generation. In *ACMMM*, pages 4204–4213, 2022.

[17] Rongjie Li, Songyang Zhang, Dahua Lin, Kai Chen, and Xuming He. From pixels to graphs: Open-vocabulary scene graph generation with vision-language models. In *CVPR*, pages 28076–28086, 2024.

[18] Tsung-Yi Lin, Michael Maire, Serge Belongie, James Hays, Pietro Perona, Deva Ramanan, Piotr Dollár, and C Lawrence Zitnick. Microsoft coco: Common objects in context. In *ECCV*, pages 740–755, 2014.

[19] Xin Lin, Changxing Ding, Jinquan Zeng, and Dacheng Tao. Gps-net: Graph property sensing network for scene graph generation. In *CVPR*, pages 3746–3753, 2020.

[20] Chen Lin, Shuai Zheng, Zhizhe Liu, Youru Li, Zhenfeng Zhu, and Yao Zhao. Sgt: Scene graph-guided transformer for surgical report generation. In *MICCAI*, pages 507–518, 2022.

[21] Haotian Liu, Chunyuan Li, Yuheng Li, and Yong Jae Lee. Improved baselines with visual instruction tuning, 2023.

[22] Ilya Loshchilov and Frank Hutter. Decoupled weight decay regularization. In *ICLR*, 2019.

[23] Yang Miao, Francis Engelmann, Olga Vysotska, Federico Tombari, Marc Pollefeys, and Dániel Béla Baráth. SceneGraphLoc: Cross-Modal Coarse Visual Localization on 3D Scene Graphs. In *ECCV*, 2024.

[24] Ege Özsoy, Evin Pinar Örnek, Ulrich Eck, Tobias Czempiel, Federico Tombari, and Nassir Navab. 4d-or: Semantic scene graphs for or domain modeling. In *MICCAI*, pages 475–485, 2022.

[25] Machel Reid, Nikolay Savinov, Denis Teplyashin, Dmitry Lepikhin, Timothy Lillicrap, Jean-baptiste Alayrac, Radu Soricu, Angeliki Lazaridou, Orhan Firat, Julian Schrittweiser, et al. Gemini 1.5: Unlocking multimodal understanding across millions of tokens of context. *arXiv preprint arXiv:2403.05530*, 2024.

[26] Shaoqing Ren, Kaiming He, Ross Girshick, and Jian Sun. Faster r-cnn: Towards real-time object detection with region proposal networks. *NeurIPS*, 28, 2015.

[27] John Schulman, Filip Wolski, Prafulla Dhariwal, Alec Radford, and Oleg Klimov. Proximal policy optimization algorithms. *arXiv preprint arXiv:1707.06347*, 2017.

[28] Zhihong Shao, Peiyi Wang, Qiiao Zhu, Runxin Xu, Junxiao Song, Xiao Bi, Haowei Zhang, Mingchuan Zhang, YK Li, Y Wu, et al. Deepseekmath: Pushing the limits of mathematical reasoning in open language models. *arXiv preprint arXiv:2402.03300*, 2024.

[29] Kaihua Tang, Hanwang Zhang, Baoyuan Wu, Wenhan Luo, and Wei Liu. Learning to compose dynamic tree structures for visual contexts. In *CVPR*, pages 6619–6628, 2019.

[30] Kaihua Tang, Yulei Niu, Jianqiang Huang, Jiaxin Shi, and Hanwang Zhang. Unbiased scene graph generation from biased training. In *CVPR*, pages 3713–3722, 2020.

[31] Leandro von Werra, Younes Belkada, Lewis Tunstall, Edward Beeching, Tristan Thrush, Nathan Lambert, Shengyi Huang, Kashif Rasul, and Quentin Gallouédec. Trl: Transformer reinforcement learning. <https://github.com/huggingface/trl>, 2020.

[32] Peng Wang, Shuai Bai, Sinan Tan, Shijie Wang, Zhihao Fan, Jinze Bai, Keqin Chen, Xuejing Liu, Jialin Wang, Wenbin Ge, Yang Fan, Kai Dang, Mengfei Du, Xuancheng Ren, Rui Men, Dayiheng Liu, Chang Zhou, Jingren Zhou, and Junyang Lin. Qwen2-vl: Enhancing vision-language model’s perception of the world at any resolution. *arXiv preprint arXiv:2409.12191*, 2024.

[33] Weiyun Wang, Yiming Ren, Haowen Luo, Tiantong Li, Chenxiang Yan, Zhe Chen, Wenhai Wang, Qingyun Li, Lewei Lu, Xizhou Zhu, et al. The all-seeing project v2: Towards general relation comprehension of the open world. In *ECCV*, pages 471–490. Springer, 2024.

[34] Danfei Xu, Yuke Zhu, Christopher B. Choy, and Li Fei-Fei. Scene graph generation by iterative message passing. In *CVPR*, pages 3097–3106, 2017.

[35] Mingjie Xu, Mengyang Wu, Yuzhi Zhao, Jason Chun Lok Li, and Weifeng Ou. Llava-spacesgg: Visual instruct tuning for open-vocabulary scene graph generation with enhanced spatial relations. In *WACV*, pages 6362–6372, 2025.

[36] Jingkang Yang, Yi Zhe Ang, Zujin Guo, Kaiyang Zhou, Wayne Zhang, and Ziwei Liu. Panoptic scene graph generation. In *ECCV*, pages 178–196. Springer, 2022.

[37] Hang Yin, Xiuwei Xu, Zhenyu Wu, Jie Zhou, and Jiwen Lu. Sg-nav: Online 3d scene graph prompting for llm-based zero-shot object navigation. *NeurIPS*, 37:5285–5307, 2024.

[38] Rowan Zellers, Mark Yatskar, Sam Thomson, and Yejin Choi. Neural motifs: Scene graph parsing with global context. In *CVPR*, pages 5831–5840, 2018.

- [39] Zhiyuan Zeng, Qinyuan Cheng, Zhangyue Yin, Yunhua Zhou, and Xipeng Qiu. Revisiting the test-time scaling of o1-like models: Do they truly possess test-time scaling capabilities? *arXiv preprint arXiv:2502.12215*, 2025.
- [40] Yong Zhang, Yingwei Pan, Ting Yao, Rui Huang, Tao Mei, and Chang Wen Chen. Learning to generate language-supervised and open-vocabulary scene graph using pre-trained visual-semantic space. In *CVPR*, pages 2915–2924, 2023.
- [41] Chenyangguang Zhang, Alexandros Delitzas, Fangjinhua Wang, Ruida Zhang, Xiangyang Ji, Marc Pollefeys, and Francis Engelmann. Open-vocabulary functional 3d scene graphs for real-world indoor spaces. In *CVPR*, 2025.
- [42] Chengyang Zhao, Yikang Shen, Zhenfang Chen, Mingyu Ding, and Chuang Gan. Textpsg: Panoptic scene graph generation from textual descriptions. In *ICCV*, pages 2839–2850, 2023.
- [43] Yiwu Zhong, Jing Shi, Jianwei Yang, Chenliang Xu, and Yin Li. Learning to generate scene graph from natural language supervision. In *ICCV*, pages 1823–1834, 2021.
- [44] Yifeng Zhu, Jonathan Tremblay, Stan Birchfield, and Yuke Zhu. Hierarchical planning for long-horizon manipulation with geometric and symbolic scene graphs. In *ICRA*, pages 6541–6548, 2021.

Table 5: Prompting an M-LLM to generate scene graphs without providing predefined object classes or predicate types.

```
messages = [{ "role": "system", "content": " {system_prompt}" }, { "role": "user", "content": f"""Generate a structured scene graph for an image using the following format: {"json { \"objects\": [ {\"id\": \"object_name.number\", \"bbox\": [x1, y1, x2, y2]}, ... ], \"relationships\": [ {\"subject\": \"object_name.number\", \"predicate\": \"relationship_type\", \"object\": \"object_name.number\"}, ... ] }\". ### **Guidelines:** - **Objects:** - Assign a unique ID for each object using the format "object_name.number" (e.g., "person.1", "bike.2"). - Provide its bounding box '[x1, y1, x2, y2]' in integer pixel format. - Include all visible objects, even if they have no relationships. - **Relationships:** - Represent interactions accurately using "subject", "predicate", and "object". - Omit relationships for orphan objects. ### **Example Output:** {"json { \"objects\": [ {\"id\": \"person.1\", \"bbox\": [120, 200, 350, 700]}, {\"id\": \"bike.2\", \"bbox\": [100, 600, 400, 800]}, {\"id\": \"helmet.3\", \"bbox\": [150, 150, 280, 240]}, {\"id\": \"tree.4\", \"bbox\": [500, 100, 750, 700]} ], \"relationships\": [ {\"subject\": \"person.1\", \"predicate\": \"riding\", \"object\": \"bike.2\"}, {\"subject\": \"person.1\", \"predicate\": \"wearing\", \"object\": \"helmet.3\"} ] }\" Now, generate the complete scene graph for the provided image: """ } ] }
```

Table 6: Prompting an M-LLM to generate scene graphs with predefined object classes and predicate types. Here, *OBJ\_CLS* and *REL\_CLS* refer to the predefined object classes and relation categories respectively.

```
messages = [{ "role": "system", "content": " {system_prompt}" }, { "role": "user", "content": f"""Generate a structured scene graph for an image using the following format: {"json { \"objects\": [ {\"id\": \"object_name.number\", \"bbox\": [x1, y1, x2, y2]}, ... ], \"relationships\": [ {\"subject\": \"object_name.number\", \"predicate\": \"relationship_type\", \"object\": \"object_name.number\"}, ... ] }\". ### **Guidelines:** - **Objects:** - Assign a unique ID for each object using the format "object_name.number" (e.g., "person.1", "bike.2"). The **object_name** must belong to the predefined object set: '{OBJ_CLS}'. - Provide its bounding box '[x1, y1, x2, y2]' in integer pixel format. - Include all visible objects, even if they have no relationships. - **Relationships:** - Represent interactions accurately using "subject", "predicate", and "object". - Omit relationships for orphan objects. - The **predicate** must belong to the predefined relationship set: '{REL_CLS}'. ### **Example Output:** {"json { \"objects\": [ {\"id\": \"person.1\", \"bbox\": [120, 200, 350, 700]}, {\"id\": \"bike.2\", \"bbox\": [100, 600, 400, 800]}, {\"id\": \"helmet.3\", \"bbox\": [150, 150, 280, 240]}, {\"id\": \"tree.4\", \"bbox\": [500, 100, 750, 700]} ], \"relationships\": [ {\"subject\": \"person.1\", \"predicate\": \"riding\", \"object\": \"bike.2\"}, {\"subject\": \"person.1\", \"predicate\": \"wearing\", \"object\": \"helmet.3\"} ] }\" Now, generate the complete scene graph for the provided image: """ } ] }
```

## A Supplementary Material

### A.1 Prompt Templates for SGG

In this work, we adopt two prompt templates for scene graph generation, as illustrated in Table 6 and Table 5. The difference lies in whether predefined object classes and relation categories are provided.

### A.2 How Well Do M-LLMs Reason About Visual Relationships?

To evaluate the reasoning capabilities of M-LLMs over visual relationships, we present results in Table 7. We vary both the visual input and the text prompt conditions to assess robustness. For visual variations, we consider: *org. img.*, *mask img.*, and *mask obj.*; for prompt variations, we add: *w/o cats*. (without object categories) and *w/o box*. (without bounding boxes).

Table 7: Comparison of VQA on the VG150 validation set across various models and settings. Gains compared to the *Original Image* (1st row) are indicated in red. “*mask img.*” refers to masking the entire image with random noise, “*mask obj.*” refers to masking object regions with black pixels, “*w/o cats.*” refers to not providing object categories in the prompt, and “*w/o box.*” refers to not providing bounding boxes in the prompt.

	InstructBLIP 7B		LLaVA v1.5 7B		LLaVA v1.6 7B		Qwen2VL 7B	
	Acc	mAcc	Acc	mAcc	Acc	mAcc	Acc	mAcc
org. img.	2.3	1.9	45.8	45.6	28.7	29.2	53.7	53.4
mask img.	1.0 <small>(-1.3)</small>	1.0 <small>(-0.9)</small>	21.8 <small>(-24.0)</small>	21.6 <small>(-24.0)</small>	3.9 <small>(-24.8)</small>	4.0 <small>(-25.2)</small>	0.0 <small>(-53.7)</small>	0.0 <small>(-53.4)</small>
mask obj.	1.9 <small>(-0.4)</small>	1.9 <small>(-0.1)</small>	37.2 <small>(-8.6)</small>	37.2 <small>(-8.4)</small>	12.8 <small>(-15.9)</small>	13.2 <small>(-16.0)</small>	16.2 <small>(-37.5)</small>	16.8 <small>(-36.5)</small>
w/o cats.	2.5 <small>(+0.2)</small>	2.4 <small>(+0.4)</small>	32.8 <small>(-12.9)</small>	32.7 <small>(-12.9)</small>	9.5 <small>(-19.2)</small>	10.1 <small>(-19.1)</small>	16.8 <small>(-36.9)</small>	18.1 <small>(-35.3)</small>
+ mask img.	1.0 <small>(-1.3)</small>	1.0 <small>(-0.9)</small>	15.4 <small>(-30.3)</small>	15.3 <small>(-30.3)</small>	0.0 <small>(-28.7)</small>	0.0 <small>(-29.2)</small>	0.2 <small>(-53.6)</small>	0.2 <small>(-53.1)</small>
+ mask obj.	1.8 <small>(-0.5)</small>	1.7 <small>(-0.3)</small>	27.9 <small>(-17.8)</small>	28.4 <small>(-17.2)</small>	3.3 <small>(-25.4)</small>	3.8 <small>(-25.4)</small>	4.7 <small>(-49.1)</small>	5.5 <small>(-47.8)</small>
w/o box.	26.0 <small>(+23.7)</small>	25.9 <small>(+24.0)</small>	61.9 <small>(+16.2)</small>	61.3 <small>(+15.7)</small>	53.5 <small>(+24.8)</small>	52.1 <small>(+22.9)</small>	78.1 <small>(+24.4)</small>	77.1 <small>(+23.8)</small>
+ mask img.	10.1 <small>(+7.9)</small>	10.2 <small>(+8.2)</small>	36.3 <small>(-9.5)</small>	35.2 <small>(-10.4)</small>	11.5 <small>(-17.2)</small>	11.4 <small>(-17.7)</small>	0.0 <small>(-53.7)</small>	0.0 <small>(-53.4)</small>
+ mask obj.	19.3 <small>(+17.0)</small>	19.1 <small>(+17.1)</small>	54.2 <small>(+8.5)</small>	53.8 <small>(+8.2)</small>	33.5 <small>(+4.8)</small>	33.2 <small>(+4.1)</small>	40.3 <small>(-13.4)</small>	39.3 <small>(-14.1)</small>

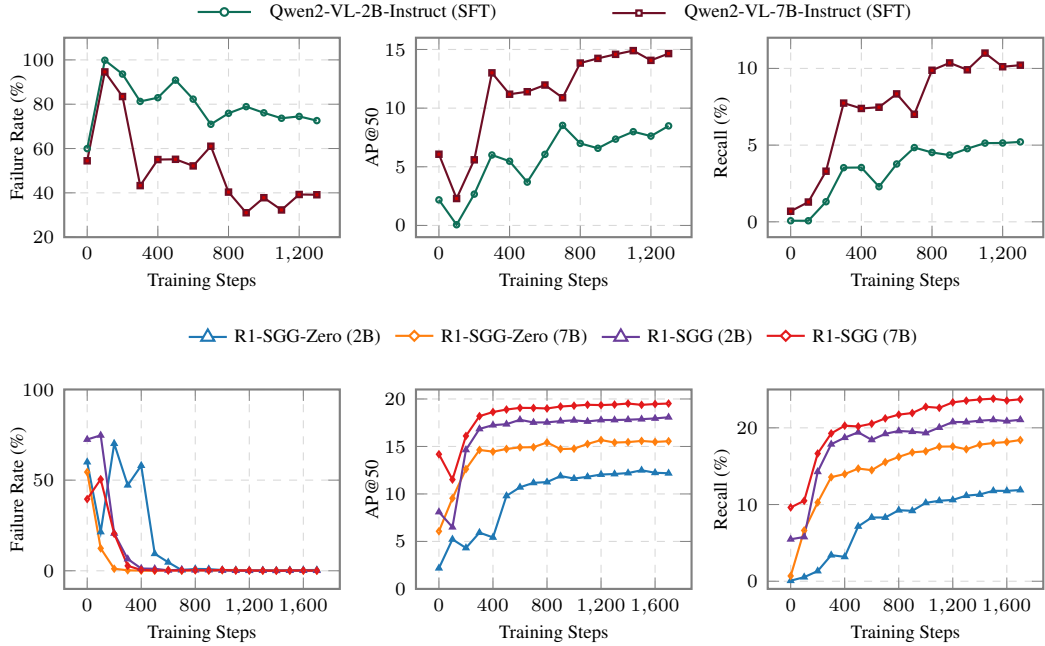
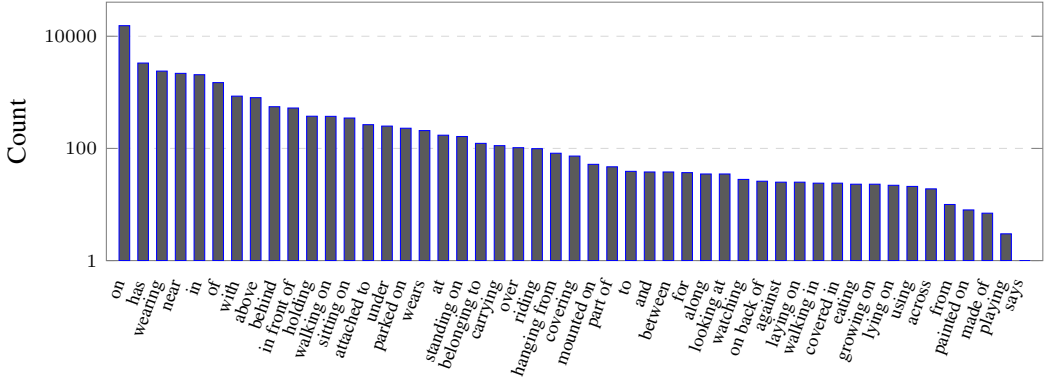


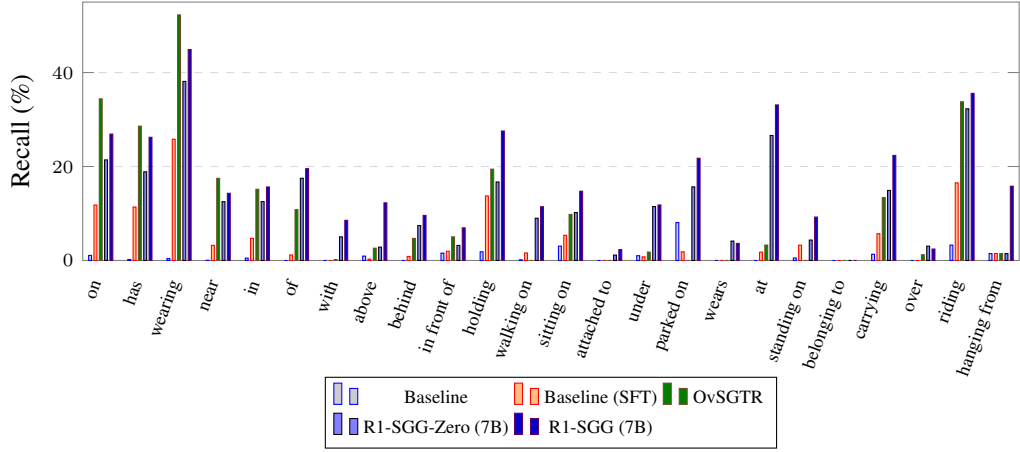
Figure 2: Comparison of R1-SGG-Zero and R1-SGG models against SFT baselines (Qwen2-VL-2B/7B-Instruct) across training steps on the VG150 validation set in terms of Failure Rate (%), AP@50, and Recall (%).

### A.3 Qualitative Results

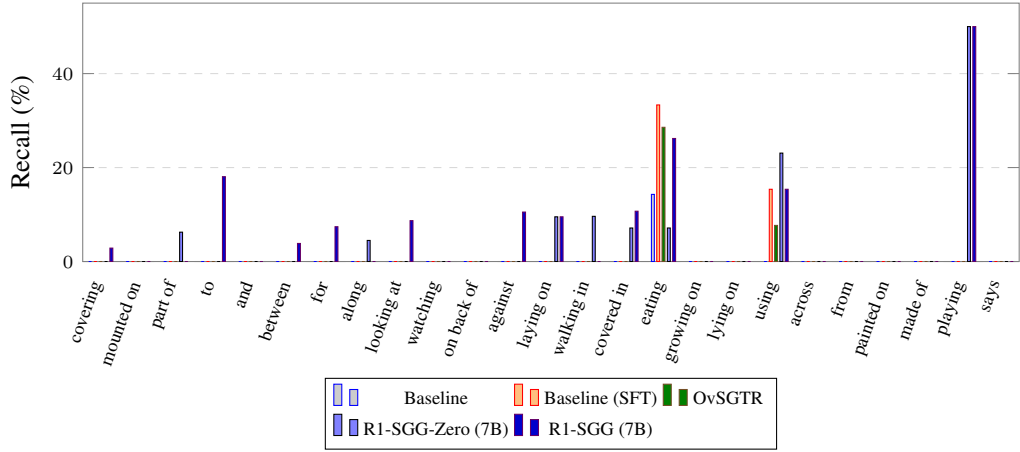
We present qualitative results in Fig. 6 and Fig. 7, and analyze head and tail predicate performance in Fig. 3 and Fig. 4 to assess long-tail bias. As shown in Fig. 3, both specific models such as OvSGTR and M-LLMs like Qwen2-VL-7B-Instruct (with or without SFT) tend to be biased toward head classes, whereas R1-SGG achieves significantly higher recall on tail predicates. This trend is also confirmed on the PSG dataset in Fig. 4. These results demonstrate that R1-SGG is more effective at generating unbiased scene graphs.



(a) Histogram of predicate frequency in the VG150 validation set.

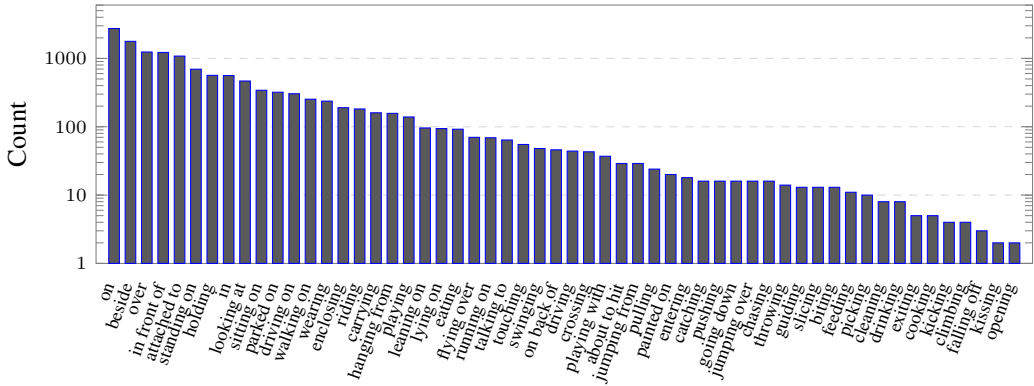


(b) Recall scores of top-24 predicates of the VG150 validation set.

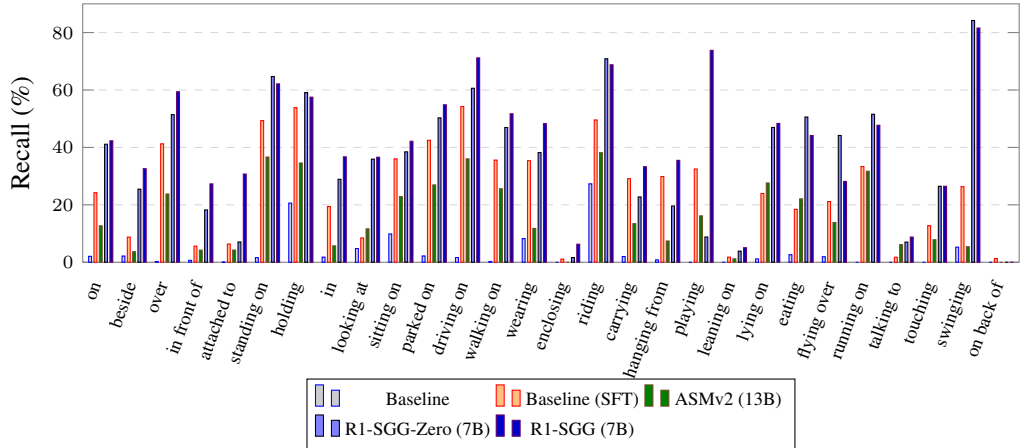


(c) Recall scores of tail-25 predicates of the VG150 validation set.

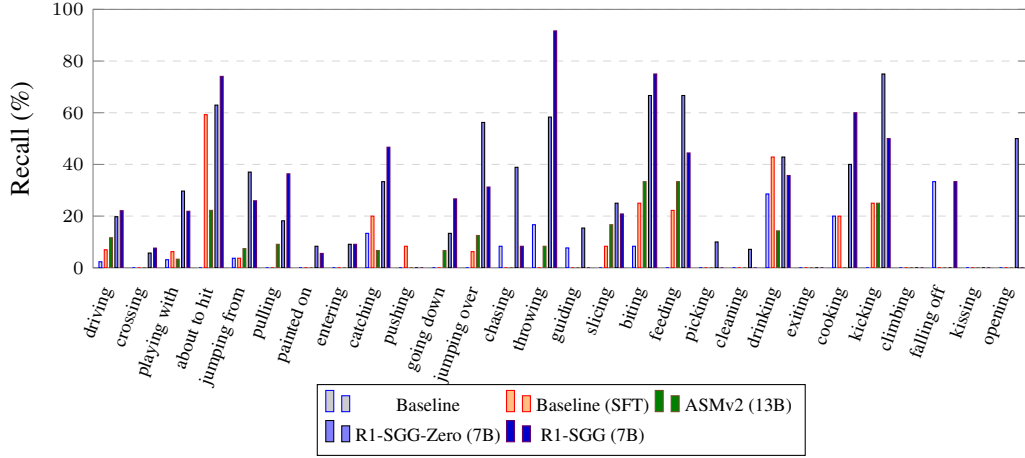
Figure 3: Comparison of predicate frequency and predicate-wise recall on the VG150 validation set. Subfigures (b) and (c) report the recall performance of *R1-SGG* compared to four models on the top-24 and tail-25 predicates (the VG150 validation set contains only 49 predicates, with the predicate “flying in” missing.), respectively. Here, *Baseline* refers to Qwen2-VL-7B-Instruct.



(a) Histogram of predicate frequency in the PSG test set.



(b) Recall scores of top-28 predicates of the PSG test set.



(c) Recall scores of tail-28 predicates of the PSG test set.

Figure 4: Comparison of predicate frequency and predicate-wise recall on the PSG test set. Subfigures (b) and (c) report the recall performance of *R1-SGG* compared to four models on the top-28 and tail-28 predicates, respectively. Here, *Baseline* refers to *Qwen2-VL-7B-Instruct*.

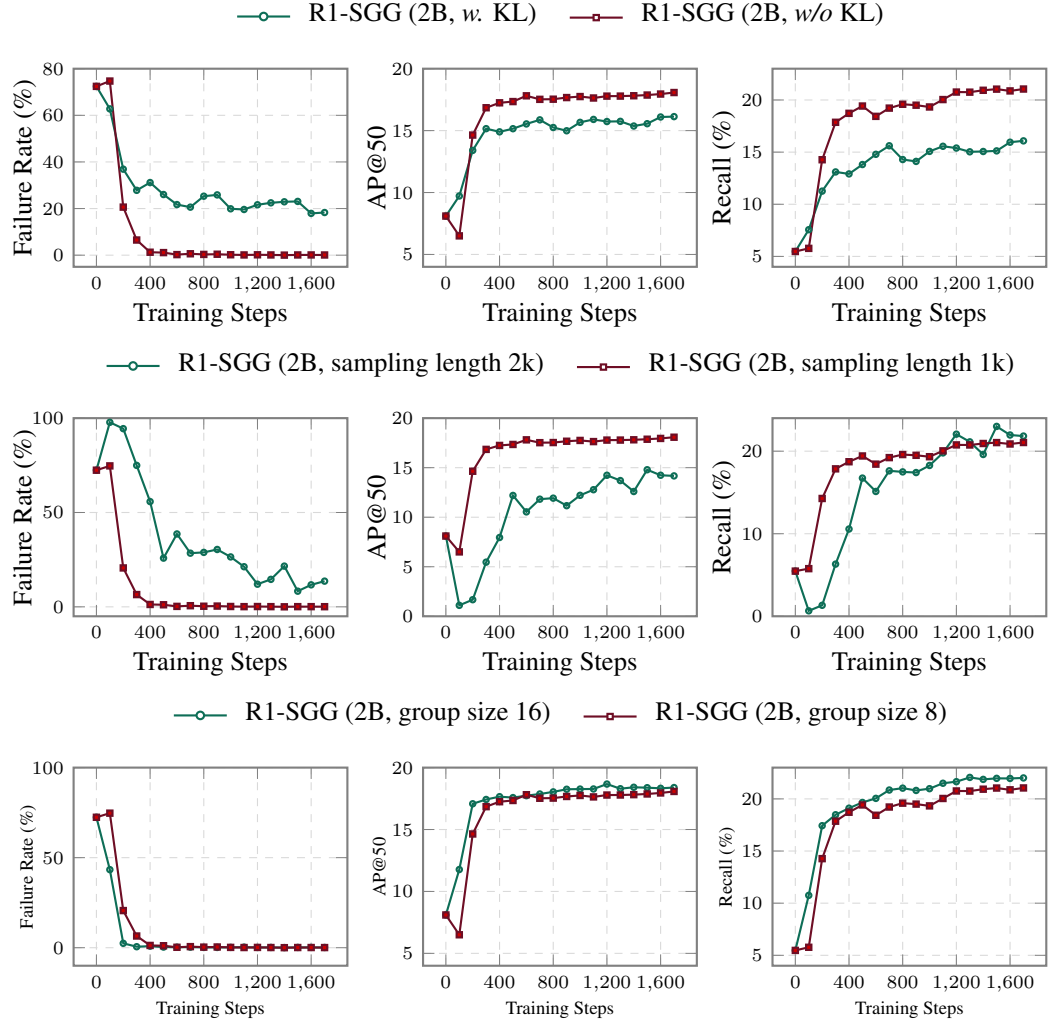
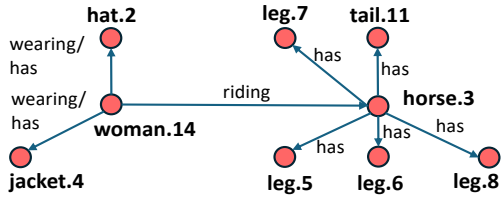
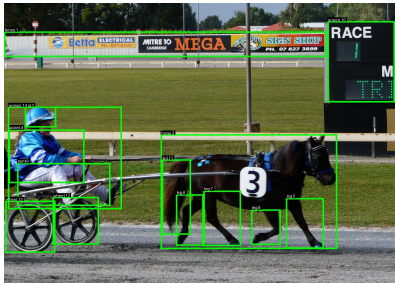


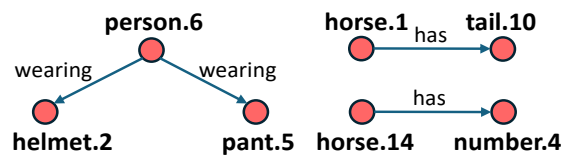
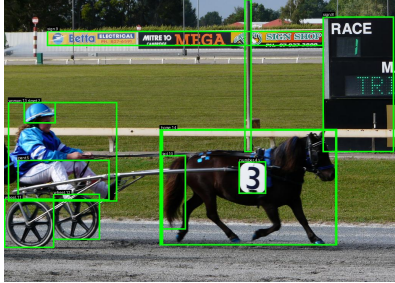
Figure 5: Performance comparison of R1-SGG (2B) across training steps on the VG150 validation set. Each row evaluates a different setting: (Top) KL divergence regularization ( $\beta=0.04$  vs.  $\beta=0$ ), (Middle) sampling length, and (Bottom) group size. Metrics reported include Failure Rate (%), AP@50, and Recall (%).



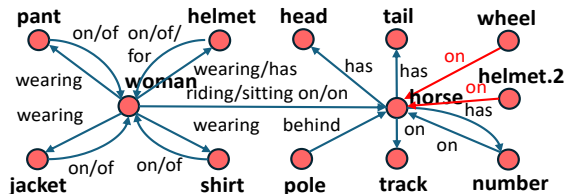
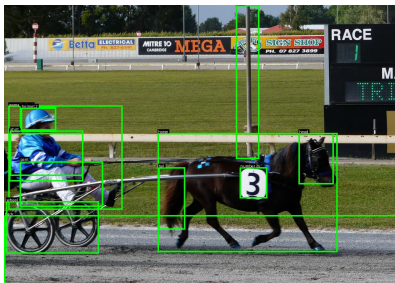
(a) GT



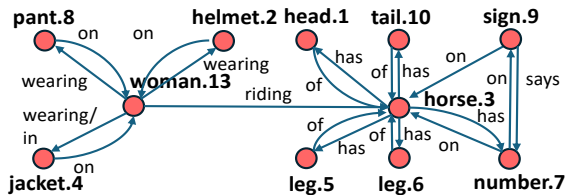
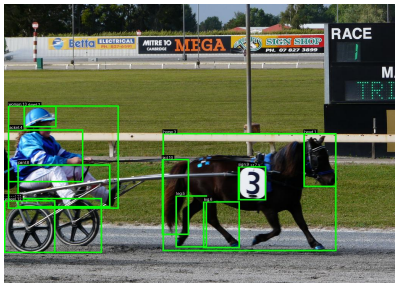
(b) Qwen2-VL-7B-Instruct.



(c) Qwen2-VL-7B-Instruct (SFT).

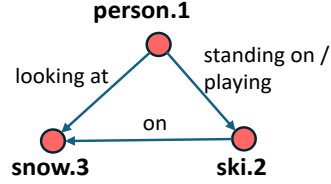
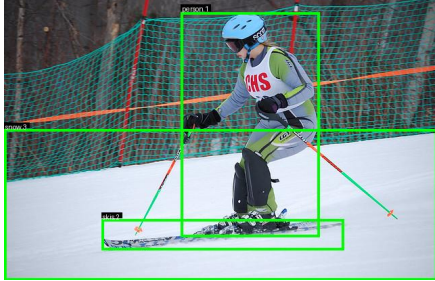


(d) R1-SGG-Zero (7B).

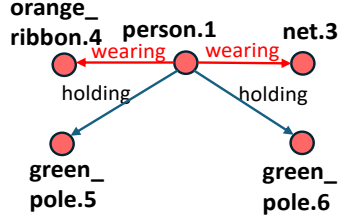
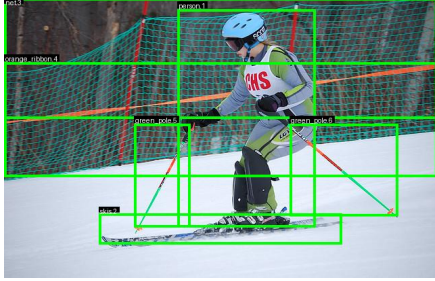


(e) R1-SGG (7B).

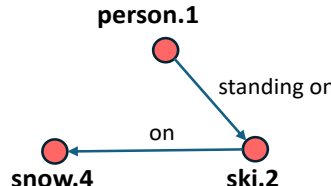
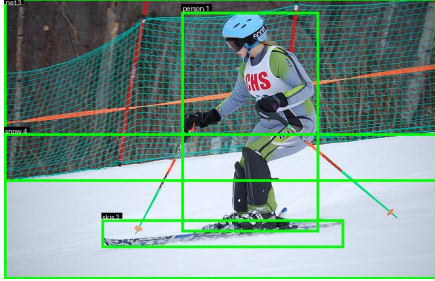
Figure 6: Qualitative comparison of generated scene graphs (from VG150). (a) Ground-truth scene graph annotated by humans. (b) Zero-shot Qwen2-VL-7B-Instruct produces an invalid JSON (failure to follow format). (c) Qwen2-VL-7B-Instruct (SFT) outputs a valid graph but omits many relations. (d) R1-SGG-Zero (7B) recovers most objects and relations but still hallucinates incorrect triplets (*e.g.*,  $\langle$  *wheel*, *on*, *horse*  $\rangle$  and  $\langle$  *helmet.2*, *on*, *horse*  $\rangle$ ). (e) R1-SGG (7B) yields a complete, structurally correct scene graph with higher recall.



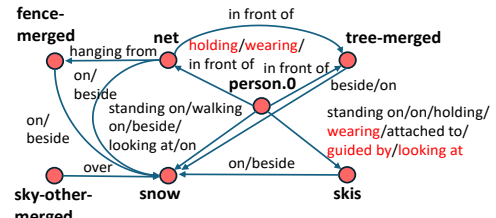
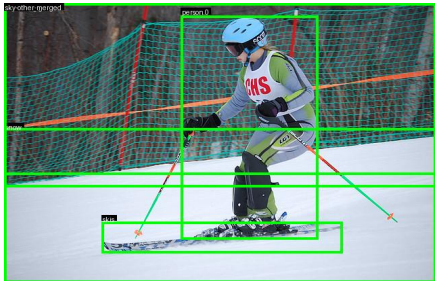
(a) GT.



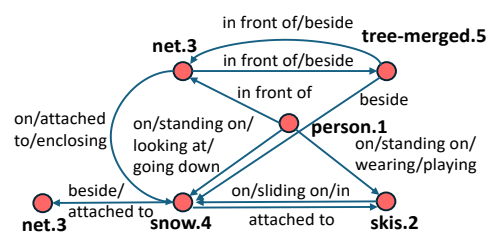
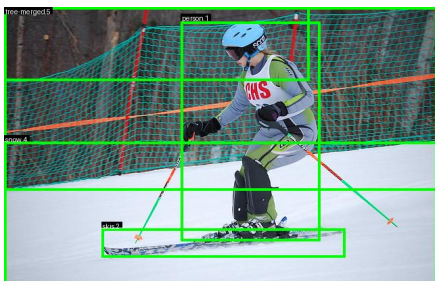
(b) Qwen2-VL-7B-Instruct.



(c) Qwen2-VL-7B-Instruct (SFT).



(d) R1-SGG-Zero (7B).



(e) R1-SGG (7B).

Figure 7: Qualitative comparison of generated scene graphs (from PSG). (a) Ground-truth scene graph annotated by humans. (b) Zero-shot Qwen2-VL-7B-Instruct generates a valid graph but includes incorrect triplets (e.g.,  $\langle person.1, wearing, net.3 \rangle$ ). (c) Qwen2-VL-7B-Instruct (SFT) produces a valid graph but omits some relationships. (d) R1-SGG-Zero (7B) recovers most objects and relations but still hallucinates errors (e.g.,  $\langle person.0, wearing, net \rangle$ ). (e) R1-SGG (7B) generates a complete and accurate scene graph with higher recall.